

Time Varying Factor Model: An Empirical Application to the European Area

Gloria Carloni, Luca Marchesi, Luca Orlando, Tommaso Zipoli¹

¹University of Bologna

November 13, 2025

Abstract

This paper applies the time-varying factor model proposed by Su and Wang (2017) to a large European macro-financial dataset in order to explore how the structure and transmission of common forces in the euro area have evolved over time. By allowing factor loadings to change smoothly, the model captures gradual shifts in the underlying economic and financial relationships.

We investigate both the dynamics and the dimensionality of the common component, showing that the number and strength of latent factors are not constant but vary across periods. In particular, the analysis highlights how the global financial crisis of 2008 and the COVID-19 pandemic in 2020 reshaped the configuration of euro-area factors. The estimated loadings reveal clear changes in the way macroeconomic and financial variables comove during these major shocks, indicating that the structure of the European business and financial cycles is itself time-dependent.

1 Introduction

Traditional static factor models, such as those developed by Stock and Watson (2002) and Bai and Ng (2002), assume that the relationships between observable variables and latent factors remain constant over time. While this assumption simplifies estimation, it may be too restrictive when data are high-dimensional or span long periods, potentially encompassing structural changes. In particular, the European economy has undergone major transformations over the past two decades, including the global financial crisis, the sovereign debt crisis, and the COVID-19 pandemic. These events likely altered the way in which common forces drive macroeconomic and financial variables across countries and sectors.

We adopt the *time-varying factor model* proposed by Su and Wang (2017), which extends the standard framework by allowing factor loadings to evolve smoothly over time. This approach combines kernel weighting and local principal component analysis (PCA) to estimate loadings and factors within a moving neighborhood around each point in time. By doing so, it captures gradual shifts in the structure of co-movements that a static model would fail to detect. Su and Wang also propose a statistical test to verify whether the assumption of time-invariant loadings can be rejected, providing a formal assessment of the presence of time variation.

We apply this methodology to a large European dataset consisting of 47 macro-financial variables and nearly 300 monthly observations from 2000 to 2023. The database covers a wide range of indicators—including national accounts, labour market, credit, price, interest rate, and monetary aggregates—compiled from institutional sources such as Eurostat, the European Central Bank, and the OECD. All series are transformed and standardized to ensure stationarity and comparability across units.

As an extension of the original framework, we allow the number of factors to vary across time and select it locally using the ABC criterion of Alessi (2010). This flexible specification enables us to assess both the evolving strength and dimensionality of the common component. The formal test strongly rejects the null hypothesis of constant loadings ($p < 0.01$), indicating that the underlying relationships among variables change significantly over time.

Our analysis focuses on the dynamics of the first two factors. The results reveal substantial time variation in their loadings, particularly around the 2008 global financial crisis and the 2020 COVID-19 shock. These findings suggest that the transmission mechanisms of macro-financial fluctuations in the euro area are not static but evolve with changing economic regimes, monetary conditions, and policy responses.

2 Methodology

We follow the framework of a *time-varying factor model* as introduced by Su and Wang (2017), which generalizes the conventional static factor model by allowing the factor loadings to evolve smoothly over time.

2.1 Model setup

Let $X_t = (X_{1t}, X_{2t}, \dots, X_{Nt})'$ denote an $N \times 1$ vector of observed variables at time t , for $t = 1, \dots, T$. The model assumes that each observable series can be decomposed as

$$X_{it} = \lambda'_{it} F_t + e_{it}, \quad i = 1, \dots, N, \quad (2.1)$$

where:

- $F_t = (F_{1t}, F_{2t}, \dots, F_{Rt})'$ is an $R \times 1$ vector of latent *common factors*;
- $\lambda_{it} = (\lambda_{i1t}, \dots, \lambda_{iRt})'$ is an $R \times 1$ vector of *factor loadings*, varying smoothly with time;
- e_{it} is an idiosyncratic error term, weakly dependent across both i and t .

In matrix form, for each period t :

$$X_t = \Lambda_t F_t + e_t, \quad (2.2)$$

where:

$$\Lambda_t = \begin{bmatrix} \lambda_{11t} & \lambda_{12t} & \cdots & \lambda_{1Rt} \\ \lambda_{21t} & \lambda_{22t} & \cdots & \lambda_{2Rt} \\ \vdots & \vdots & \ddots & \vdots \\ \lambda_{N1t} & \lambda_{N2t} & \cdots & \lambda_{NRt} \end{bmatrix}_{N \times R}, \quad F_t = \begin{bmatrix} F_{1t} \\ F_{2t} \\ \vdots \\ F_{Rt} \end{bmatrix}_{R \times 1}, \quad e_t = \begin{bmatrix} e_{1t} \\ e_{2t} \\ \vdots \\ e_{Nt} \end{bmatrix}_{N \times 1}.$$

Stacking all T observations, the full dataset can be written as:

$$X = F \Lambda' + E, \quad (2.3)$$

where:

$$X = \begin{bmatrix} X'_1 \\ X'_2 \\ \vdots \\ X'_T \end{bmatrix}_{T \times N}, \quad F = \begin{bmatrix} F'_1 \\ F'_2 \\ \vdots \\ F'_T \end{bmatrix}_{T \times R}, \quad \Lambda' = \begin{bmatrix} \lambda_{11} & \lambda_{21} & \cdots & \lambda_{N1} \\ \lambda_{12} & \lambda_{22} & \cdots & \lambda_{N2} \\ \vdots & \vdots & \ddots & \vdots \\ \lambda_{1R} & \lambda_{2R} & \cdots & \lambda_{NR} \end{bmatrix}_{R \times N}, \quad E = \begin{bmatrix} e'_1 \\ e'_2 \\ \vdots \\ e'_T \end{bmatrix}_{T \times N}.$$

2.2 Time-varying structure

To capture gradual structural changes, the loadings are modeled as smooth functions of rescaled time:

$$\lambda_{it} = \lambda_i(\tau_t), \quad \text{where } \tau_t = \frac{t}{T}, \quad \tau_t \in (0, 1]. \quad (2.4)$$

Hence, each $\lambda_i(\cdot)$ represents a smooth curve describing how the loading of variable i on each factor evolves throughout the sample.

This specification allows the model to account for long-term transitions—such as technological progress, financial integration, or policy regime shifts—without imposing discrete breaks.

2.3 Identification

Similarly to the conventional version of a factor model, the loadings and factors are not independently identifiable by the estimation procedure—i.e. we have $\lambda'_{it} F_t = (H_t^{-1} \lambda_{it})'(H_t' F_t)$ for any $R \times R$ nonsingular matrix H_t —unless imposing R^2 restrictions. Following Bai and Ng (2002), we impose normalization restrictions to remove rotational indeterminacy:

$$\frac{1}{T} F' F = I_R, \quad \frac{1}{N} \Lambda'_t \Lambda_t = \text{diag}(c_1(\tau_t), \dots, c_R(\tau_t)), \quad (2.5)$$

where $c_r(\tau_t)$ denotes the time-varying strength of the r -th factor at time τ_t .

These constraints ensure that the scale and rotation of factors and loadings are uniquely identified at each point in time.

2.4 Objective

Within this framework, the main goal is to describe how the *common component*:

$$\chi_{it} = \lambda'_{it} F_t$$

evolves over time, and to determine whether changes in the factor loadings represent genuine structural shifts in the data-generating process or gradual regime adaptations.

The subsequent section details the estimation of the local factors and loadings using a kernel-weighted version of principal component analysis (PCA), as proposed by Su and Wang (2017).

3 Estimation

In this section, we estimate the time-varying factor loadings and common factors by implementing a local version of principal component analysis (PCA), following the approach proposed by Su and Wang (2017). The underlying assumption is that the factor loadings $\lambda_i(\cdot)$ are smooth functions of time, so that within a small local neighborhood around $\tau = r/T$ they can be approximated by constants. Accordingly, the high-dimensional factor model

$$X_{it} = \lambda'_{it} F_t + e_{it}, \quad i = 1, \dots, N, \quad t = 1, \dots, T, \quad (3.1)$$

can be locally approximated by

$$X_{it} \approx \lambda'_{ir} F_t + e_{it}, \quad \text{for } t \approx r, \quad (3.2)$$

where λ_{ir} denotes the local loading evaluated at the rescaled time $\tau = r/T$.

To obtain the local estimates $\{\lambda_{ir}\}_{i=1}^N$ and $\{F_t\}_{t=1}^T$, we consider the kernel-weighted least squares (WLS) problem

$$\min_{\{\lambda_{ir}\}, \{F_t\}} (NT)^{-1} \sum_{i=1}^N \sum_{t=1}^T (X_{it} - \lambda'_{ir} F_t)^2 K_h\left(\frac{t-r}{T}\right), \quad (3.3)$$

where $K_h(x) = h^{-1}K(x/h)$ is a rescaled kernel function, and $h = h(T, N)$ denotes the bandwidth parameter that controls the local neighborhood width. In practice, we use the **Epanechnikov kernel**,

$$K(z) = 0.75(1 - z^2)\mathbf{1}(|z| < 1), \quad (3.4)$$

and set h according to a **Silverman (1986) rule-of-thumb** adapted to the panel setting,

$$h = cT^{-1/5}N^{-1/10}, \quad \text{with } c = \frac{2.35}{\sqrt{12}}, \quad (3.5)$$

ensuring a balance between bias and variance. The effective local window is therefore defined by $\tau \in [h, 1 - h]$, so that boundary observations—where the kernel support would otherwise be truncated—are excluded from the estimation grid. This trimming avoids the need for boundary kernels as in Su and Wang (2017), while preserving the uniform order of approximation over the interior region.

For each value of τ , we define the normalized weights

$$w_t(\tau, h) = \frac{1}{h}K\left(\frac{t/T - \tau}{h}\right), \quad (3.6)$$

and construct the locally demeaned, kernel-weighted data matrix

$$X_r = W^{1/2}(X - \mu_\tau), \quad \mu_\tau = \frac{\sum_t w_t(\tau, h)X_t}{\sum_t w_t(\tau, h)}, \quad (3.7)$$

where $W^{1/2} = \text{diag}(\sqrt{w_t(\tau, h)})$. The local WLS problem is equivalent to minimizing

$$\text{tr}[(X_r - F(\tau)\Lambda(\tau)')(X_r - F(\tau)\Lambda(\tau)')'], \quad (3.8)$$

subject to the standard identification restrictions

$$F(\tau)'F(\tau)/T = I_R, \quad \Lambda(\tau)'\Lambda(\tau) = \text{diagonal}. \quad (3.9)$$

Under these constraints, the solution corresponds to the principal components of X_r . Letting $X_r X_r'$ denote the weighted covariance matrix, the estimated factors $\hat{F}(\tau)$ are given by \sqrt{T} times the eigenvectors associated with the R largest eigenvalues of $X_r X_r'$, and the local loadings are obtained as

$$\hat{\Lambda}(\tau) = \frac{X_r' \hat{F}(\tau)}{T}. \quad (3.10)$$

These local estimates provide $\hat{F}(\tau)$ and $\hat{\Lambda}(\tau)$ only up to an orthogonal rotation and sign indeterminacy. In practice, we address this by aligning the estimated loadings across the grid of τ using a **Procrustes rotation**, which ensures consistency of signs and orientation over time and prevents spurious discontinuities in the estimated loading paths.

The above procedure yields local factors and loadings that satisfy the weighted relation

$$X_t \approx \Lambda(\tau)'F_t(\tau), \quad F_t(\tau) = \sqrt{w_t(\tau, h)}F_t, \quad (3.11)$$

implying that $\hat{F}(\tau)$ identifies a kernel-weighted version of the true factors. To recover the unweighted factors F_t on their original scale, we perform a **second-stage least squares regression**. Specifically, given the first-stage estimates $\hat{\lambda}_{it}$ from local PCA, the unweighted factors at each time t are obtained by solving

$$\min_{F_t \in \mathbb{R}^R} \sum_{i=1}^N \left(X_{it} - \hat{\lambda}'_{it} F_t \right)^2, \quad (3.12)$$

which yields the closed-form expression

$$\widehat{F}_t = \left(\sum_{i=1}^N \widehat{\lambda}_{it} \widehat{\lambda}'_{it} \right)^{-1} \sum_{i=1}^N \widehat{\lambda}_{it} X_{it}. \quad (3.13)$$

This second step removes the local kernel weighting and provides consistent estimates of the common factors \widehat{F}_t up to the same rotation used in the first stage.

In summary, the estimation proceeds as follows: the first stage performs local weighted PCA to estimate $(\widehat{F}(\tau), \widehat{\Lambda}(\tau))$ within a moving window defined by the bandwidth h , while the second stage, using the consistent estimator of $\widehat{\Lambda}$, recovers the unweighted factors \widehat{F}_t through cross-sectional OLS regressions.

3.1 Determining the Number of Local Factors.

In the above estimation procedure, the number of factors R was assumed to be known. In practice, it must be determined from the data. Following Su and Wang (2017), we denote the true number of factors by R_0 , bounded above by a finite integer R_{\max} , and employ information criteria to identify it. While Su and Wang propose a local BIC-type criterion inspired by Bai and Ng (2002), we first evaluate the classical Bai–Ng criteria locally and subsequently refine them using the adaptive ABC approach of Alessi (2010).

Let $\widehat{F}_t(R)$ and $\widehat{\lambda}_{it}(R)$ denote the local PCA estimators of the factors and loadings under the assumption of R factors, obtained by imposing the normalization

$$N^{-1} \Lambda'_r(R) \Lambda_r(R) = I_R, \quad T^{-1} F^{(r)}(R)' F^{(r)}(R) = \text{diag}(d_1, \dots, d_R), \quad (3.14)$$

where the diagonal elements d_j are arranged in descending order. Define the average residual variance function

$$V(R) = \frac{1}{NT} \sum_{i=1}^N \sum_{t=1}^T \left(X_{it} - \widehat{\lambda}'_{ir}(R) \widehat{F}_t(R) \right)^2, \quad (3.15)$$

The information criteria of Bai and Ng (2002) provide a consistent method for identifying the number of factors in large-dimensional approximate factor models, under the double asymptotic regime where both N and T diverge. Bai and Ng propose three alternative criteria, denoted IC_1 , IC_2 , and IC_3 , each differing in the strength of the penalization term ρ_{NT} . While all three are asymptotically equivalent, only the first two have been found to perform satisfactorily in finite samples; the third tends to over-penalize and may underestimate the true number of factors. We therefore focus on the first two specifications.

The generic information criterion is then given by

$$\text{IC}(R) = \log V(R) + R \rho_{NT}, \quad (3.16)$$

where ρ_{NT} is the penalty term controlling the trade-off between model fit and parsimony. We consider the two empirically reliable versions:

$$\rho_{NT}^{(1)} = \frac{N + T_{\text{eff}}}{N T_{\text{eff}}} \log \left(\frac{N T_{\text{eff}}}{N + T_{\text{eff}}} \right), \quad (3.17)$$

$$\rho_{NT}^{(2)} = \frac{N + T_{\text{eff}}}{N T_{\text{eff}}} \log \left(\min \{ \sqrt{T_{\text{eff}}}, \sqrt{N} \} \right)^2, \quad (3.18)$$

where T_{eff} denotes the effective number of time observations within each local kernel window. The first penalty (3.17) corresponds to the original IC_1 criterion, based on the logarithm of the ratio between total and effective sample sizes; the second (3.18) corresponds to IC_2 , which adjusts the penalty according to the smaller dimension between T_{eff} and N . Both criteria balance

the risk of overfitting against the bias induced by local smoothing, while retaining the same asymptotic consistency.

For each localization point τ , we compute

$$\hat{R}_{IC}^{(j)}(\tau) = \arg \min_{R \leq R_{\max}} [\log V(R) + R \rho_{NT}^{(j)}], \quad j = 1, 2, \quad (3.19)$$

and store the resulting $\hat{R}_{IC}(\tau)$ along the time grid. The comparison between $\hat{R}_{IC}^{(1)}$ and $\hat{R}_{IC}^{(2)}$ provides a diagnostic check of local stability in the estimated number of factors, as both criteria are consistent for R_0 when $N, T \rightarrow \infty$.

Although the Bai–Ng criterion performs well asymptotically, its finite-sample behavior may be unstable, often leading to over-or underestimation of R_0 —see, for instance, Forni et al. (2009)—. To improve robustness, Alessi (2010) propose an adaptive modification—the ABC criterion—that introduces a tuning parameter $c > 0$ governing the penalization strength. While this modification leaves asymptotic consistency unaffected, it enhances the criterion’s sensitivity in finite samples, especially under heteroskedastic idiosyncratic components or unbalanced cross-sections.

Formally, the ABC criterion takes the form

$$IC_{ABC}(R, c) = \log V(R) + c R \rho_{NT}, \quad (3.20)$$

where c varies over a grid $\mathcal{C} = [1/c_{\max}, c_{\max}]$. For each $c \in \mathcal{C}$ and subsample size n_s (with $n_s \in [N - nbck, N]$), we compute the minimizing rank $\hat{R}_{c,n_j}^T = \arg \min_R IC_{ABC}(R, c)$. Stability with respect to both c and n_s is then assessed through the empirical variance

$$S_c = \text{Var}_{n_s}(\hat{R}_{c,n_j}^T), \quad (3.21)$$

and the selected number of factors corresponds to the most stable range of c where \hat{R}_{c,n_j}^T remains constant across subsamples.

In our implementation, we first compute $\hat{R}_{IC}(\tau)$ from the Bai–Ng criterion for each local window. We then refine it by applying the ABC procedure to the corresponding weighted matrix X_τ . The algorithm evaluates $IC_{ABC}(R, c)$ for a dense grid of c values and multiple random subsamples of cross-sectional size n_s , retaining as $\hat{R}_{ABC}(\tau)$ the value of R corresponding to the most stable plateau in the function $c \mapsto \hat{R}_{c,n_j}^T$. Graphically, this corresponds to the flat regions of the \hat{R}_{c,n_j}^T curve discussed in Alessi (2010). We notice that there are several intervals in which a plateau is reached; however following the same theoretical reasoning as in Hallin and Liška (2007), the relevant stability interval is the second—the first corresponds to R_{\max} . By construction, the ABC refinement produces smoother and more robust estimates $\hat{R}_{ABC}(\tau)$ than the standard $\hat{R}_{IC}(\tau)$, while maintaining the same large-sample consistency properties as the Bai–Ng criterion.

4 Testing the constancy of the factor loadings

Consider the approximate factor model

$$X_{it} = \lambda'_{it} F_t + e_{it}, \quad i = 1, \dots, N, \quad t = 1, \dots, T, \quad (4.1)$$

where X_t is an N -dimensional vector of observations, F_t is an R -dimensional vector of common factors, λ_{it} are the corresponding factor loadings, and e_{it} are idiosyncratic components. Under the null hypothesis the loadings are constant,

$$H_0 : \lambda_{it} = \lambda_{i0} \quad \forall t, \quad (4.2)$$

whereas under the alternative they vary smoothly with rescaled time $\tau = t/T$,

$$H_1 : \lambda_{it} = \lambda_i(\tau), \quad \text{smooth in } \tau \in (0, 1). \quad (4.3)$$

Under H_0 , the model reduces to

$$X_t = \Lambda_0 F_t + e_t, \quad (4.4)$$

with $\Lambda_0 = (\lambda_{10}, \dots, \lambda_{N0})'$ and $e_t = (e_{1t}, \dots, e_{Nt})'$. The global estimators $(\tilde{F}_t, \tilde{\Lambda}_0)$ are obtained by applying principal components to the full sample, minimizing

$$\frac{1}{NT} \sum_{t=1}^T \|X_t - \Lambda_0 F_t\|^2, \quad \text{subject to } \frac{1}{T} F' F = I_R. \quad (4.5)$$

Under this normalization, the estimated factors and loadings satisfy

$$\tilde{F} = X \tilde{\Lambda}_0 (\tilde{\Lambda}'_0 \tilde{\Lambda}_0)^{-1}, \quad \tilde{\Lambda}_0 = \frac{1}{T} X' \tilde{F}. \quad (4.6)$$

Hence, \tilde{F} corresponds to the first R eigenvectors of the covariance matrix XX'/NT , and $\tilde{\Lambda}_0$ is obtained by projecting X onto \tilde{F} . The fitted common component under H_0 is

$$\tilde{\chi}_t = \tilde{\Lambda}_0 \tilde{F}_t. \quad (4.7)$$

Under H_1 , local PCA with kernel weights

$$K_h(t/T - \tau) = \frac{1}{h} K\left(\frac{t/T - \tau}{h}\right) \quad (4.8)$$

is applied to obtain \hat{F}_t and $\hat{\lambda}_{it}$ for each $\tau \in (0, 1)$.

Let $\tilde{\chi}_{it} = \tilde{\lambda}'_{i0} \tilde{F}_t$ and $\hat{\chi}_{it} = \hat{\lambda}'_{it} \hat{F}_t$ denote, respectively, the estimated common components under the null and the alternative. The sample quadratic distance between the two is defined as

$$\hat{M} = \frac{1}{NT} \sum_{i=1}^N \sum_{t=1}^T (\hat{\chi}_{it} - \tilde{\chi}_{it})^2. \quad (4.9)$$

Define the kernel and convolution weights

$$k_{h,st} = h^{-1} K\left(\frac{s-t}{Th}\right), \quad \bar{k}_{st} = \int_{-1}^1 K(v) K\left(\frac{s-t}{Th} - v\right) dv, \quad (4.10)$$

and the bias and variance normalizers

$$B_{NT} = \frac{h^{1/2}}{N^{1/2} T^2} \sum_{i=1}^N \sum_{t=1}^T \sum_{s=1}^T (F'_t L_{st} F_s)^2 e_{is}^2, \quad (4.11)$$

$$V_{NT} = 2T^{-2} N^{-1} h^{-1} \sum_{r \neq s} \bar{k}_{sr}^2 \mathbb{E}[(F'_s H_0 \bar{\Sigma}_F H'_0 F_r)^2 (e'_{rs})^2], \quad (4.12)$$

where L_{st} collects kernel-weighted rotations from local PCA and H_0 , $\bar{\Sigma}_F$ are the population limits under H_0 .

The standardized test statistic is

$$J_{NT} = V_{NT}^{-1/2} (TN^{1/2} h^{1/2} \hat{M} - B_{NT}), \quad (4.13)$$

which converges in distribution to the standard normal,

$$J_{NT} \xrightarrow{d} \mathcal{N}(0, 1) \quad \text{under } H_0. \quad (4.14)$$

Finite-sample inference can deviate from the asymptotic approximation. Su and Wang therefore propose a bootstrap procedure that preserves both heteroskedasticity and cross-sectional dependence in the residuals. In practice, we implement this test using the **R** package **TVMVP**, which reproduces the bootstrap algorithm developed by Su and Wang (2017). This approach provides empirical critical values that account for cross-sectional dependence and finite-sample effects, ensuring more reliable inference than asymptotic approximations.

5 Data

The dataset consists exclusively of Euro Area (EA) aggregate macro-financial time series. All variables are drawn from the dataset *EA-MD-QD*, compiled from official sources such as Eurostat (EUR), the European Central Bank (ECB), the OECD, and FRED.

The database includes a comprehensive set of indicators grouped into eleven broad categories: (1) national accounts, (2) labour market indicators, (3) credit aggregates, (4) labour costs, (5) exchange rates, (6) interest rates, (7) industrial production and turnover, (8) prices, (9) confidence indicators, (10) monetary aggregates, and (11) other financial variables such as share prices and car registrations. All series are expressed in consistent units (chain-linked volumes, indices, or percentages) and are seasonally and calendar adjusted (SCA or SA) when available.

The dataset spans from 2000Q1 to 2023Q4 and primarily features **monthly** observations. Before estimation, all series were transformed to achieve stationarity. Following the procedures outlined in the file `routine_data.m`, a **light transformation** was applied to all variables.

A few remaining non-stationary series were rendered stationary through an additional first-difference transformation.

Finally, all series were standardized to have zero mean and unit variance, ensuring comparability across variables and preventing scale differences from affecting the extraction of common factors.

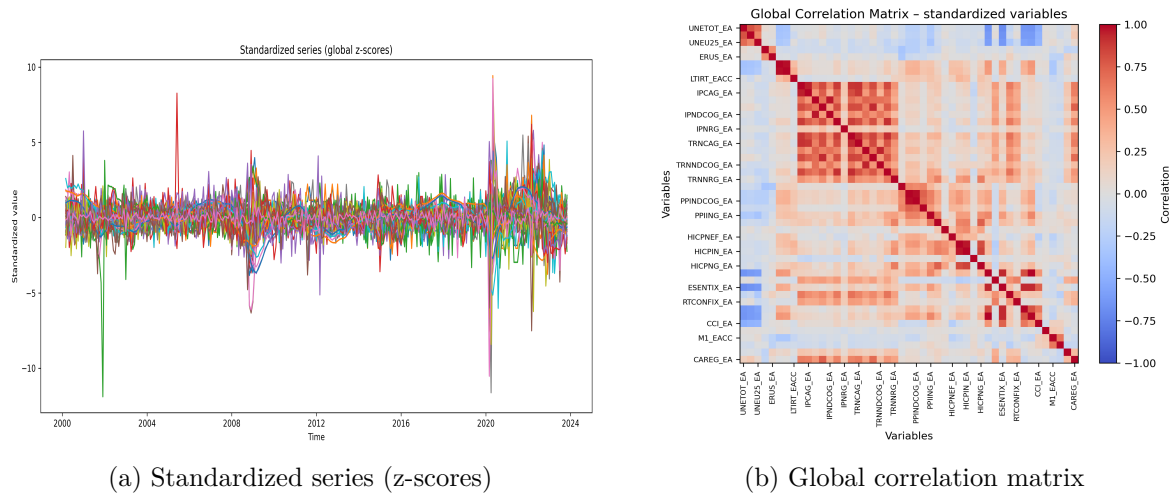
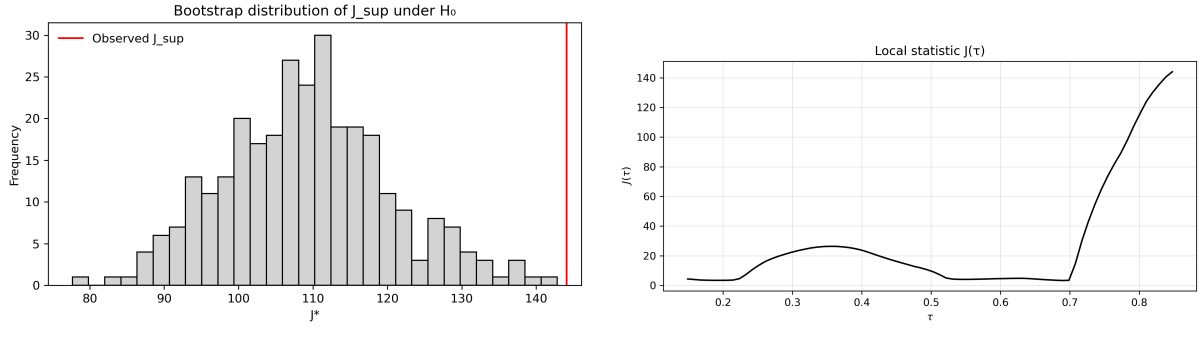


Figure 1: Overview of standardized data and correlation structure.

6 Empirical Results

6.1 Stability test



(a) Bootstrap distribution of J_{sup} under H_0 . The red line marks the observed statistic.
(b) Local statistic $J(\tau)$ across the rescaled time domain.

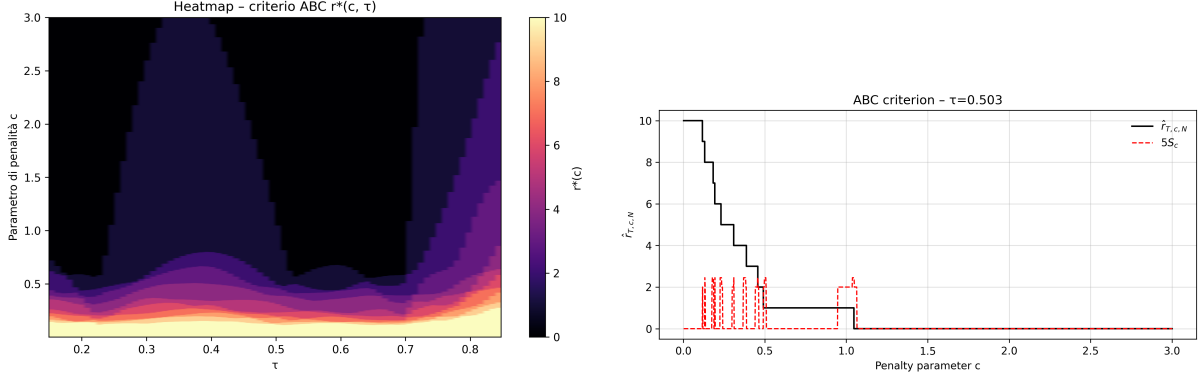
Figure 2: Bootstrap-based inference for the constancy of factor loadings. The left panel reports the simulated null distribution, while the right panel shows the local test statistic $J(\tau)$ indicating time variation.

As shown in Figure 2, the local statistic $J(\tau)$ exhibits pronounced instability, particularly in the post-COVID period, where the values rise sharply and signal strong time variation in the factor loadings. Consistently, the bootstrap distribution of J_{sup} (left panel) places the observed statistic in the far upper tail, leading to the rejection of the null hypothesis of constant loadings at conventional significance levels (the corresponding p -value is effectively zero). These findings clearly justify the adoption of a time-varying factor model, as they highlight the presence of structural shifts in the underlying relationships. Allowing the loadings to evolve over time enables us to capture how the relative contribution of each variable to the identification of the common factors changes across different economic phases, providing a more accurate and dynamic representation of the euro-area comovements.

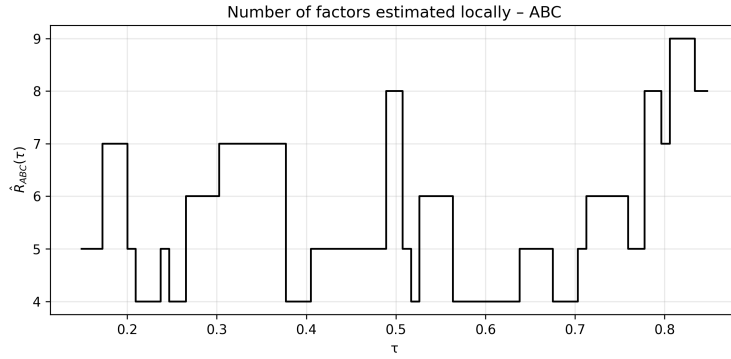
6.2 Bai-Ng and ABC

The determination of the number of factors across local windows is conducted using both standard Information Criteria by Bai and Ng (2002) and the refined ABC criterion by Alessi (2010). Our goal is a local cross-validation of factor dimensionality within the time-varying setting, so that selected factors reflect structural changes rather than sampling noise. In each window we identify stability regions – plateaux – where the empirical variance explained by the extracted components is locally constant; following Alessi (2010), persistent plateaux are taken to indicate economically meaningful latent dimensions.

To make this selection transparent, we report a heatmap of the selected factor count over the τ -grid and, for representative τ 's, window-level plots showing the stepwise changes in the estimated number of factors together with the corresponding empirical variance. As shown in Alessi (2010), due to the monotonicity of \hat{R}_{c,n_j}^T we expect the step function to display well-defined stability ranges and for moderate values of c to be a stable function of the sample size (n_j, τ_j) . The stability is furthermore illustrated by the empirical variance.



(a) Heatmap of the selected number of factors across taus, conditioned on the grid of penalties (b) \hat{R}_{c,n_j}^T and S_c as functions of c for a specific tau



(c) Selected number of factors $\hat{R}(\tau)$ over the τ -grid

Figure 3: Selection of the number of factors across local windows. The left panel shows the heatmap of the selected number of factors obtained through the refined ABC criterion over the τ -grid, depending on the penalizing parameter c . The right panel focuses on a representative τ -specific window, displaying \hat{R}_{c,n_j}^T and the corresponding scaled empirical variance S_c . The bottom panel reports $\hat{R}(\tau)$ across time, summarizing the local dimensionality.

6.3 Factors

Before discussing the estimated factors, it is important to recall that the model is based on a two-sided kernel. This specification implies that each local estimate incorporates information not only from past observations but also from future ones within the bandwidth of the kernel. As a consequence, the factors may appear to anticipate macroeconomic shocks by roughly one or two years. In reality, this apparent anticipation simply reflects the smoothing window: the kernel starts to integrate the information content of the upcoming observations before the shock fully materializes. Therefore, the dynamics shown in the figures below should be interpreted as locally smoothed representations of the underlying time-varying relationships rather than as true forecasts.

6.3.1 Interpreting the Time-Varying Loadings

Factor 1 represents an inverse real business cycle. It increases during periods of economic slowdown or monetary tightening, when the euro appreciates, unemployment rises, and monetary aggregates such as M2 expand, while industrial production and stock prices weaken. Conversely, it declines during phases of economic expansion, characterized by exchange rate depreciation, higher output, and rising asset prices. The factor therefore reflects macroeconomic stress when

positive and real expansion when negative.

During the global financial crisis (2008–2013), the loadings of **REER42** and **M2** sharply increased, while those of **IPNRG** and **SHIX** turned negative. This configuration suggests that during the crisis, the latent factor was primarily driven by the dynamics of monetary liquidity and currency value, with **M2** and **REER42** reflecting these movements, while **IPNRG** and **SHIX** captured the contraction in real activity and financial markets.

Between 2013 and 2019, the loadings of **M2** remained positive but showed a gradual decline, signaling a weakening impact of the earlier expansionary monetary policies. Conversely, **REER42** experienced a clear stability, indicating that the relationship between the euro's value and the factor became constant as the economy stabilized. During this period, **IPNRG** and **SHIX** displayed more stability, with **SHIX** moving toward a neutral position, suggesting that financial market tensions decreased as the economy entered recovery.

With the outbreak of the COVID-19 pandemic (2020–2021), the loadings of **M2** surged once again, reflecting the renewed monetary expansion. However, **REER42** started its decline, suggesting that the euro's role in the factor became even less pronounced during this period of crisis. **IPNRG** and **SHIX**, instead of becoming more negative, maintained a relatively stable or even slightly positive relationship with the factor, highlighting that real economic activity and financial markets behaved differently compared to previous crisis periods.

The **UNEU25** loading, which represents youth unemployment, became notably positive during the pandemic period, indicating that youth unemployment dynamics played an increasingly significant role in driving the common factor during the crisis. This shift underscores how labor market tensions, particularly among younger workers, became more important in shaping macro-financial dynamics during the pandemic.

Overall, Factor 1 can be interpreted as a measure of macro-financial tension, capturing the evolving influence of monetary liquidity, real economic activity, and labor market conditions. The factor tends to be positive during periods of economic distress, with high loadings for **M2** and **UNEU25**, and negative during more stable or expanding periods, where **IPNRG** and **SHIX** show stronger relationships. The time-varying nature of this factor allows us to identify shifts in the structure of macro-financial interactions, with the most significant changes occurring during the global financial crisis and the COVID-19 pandemic.

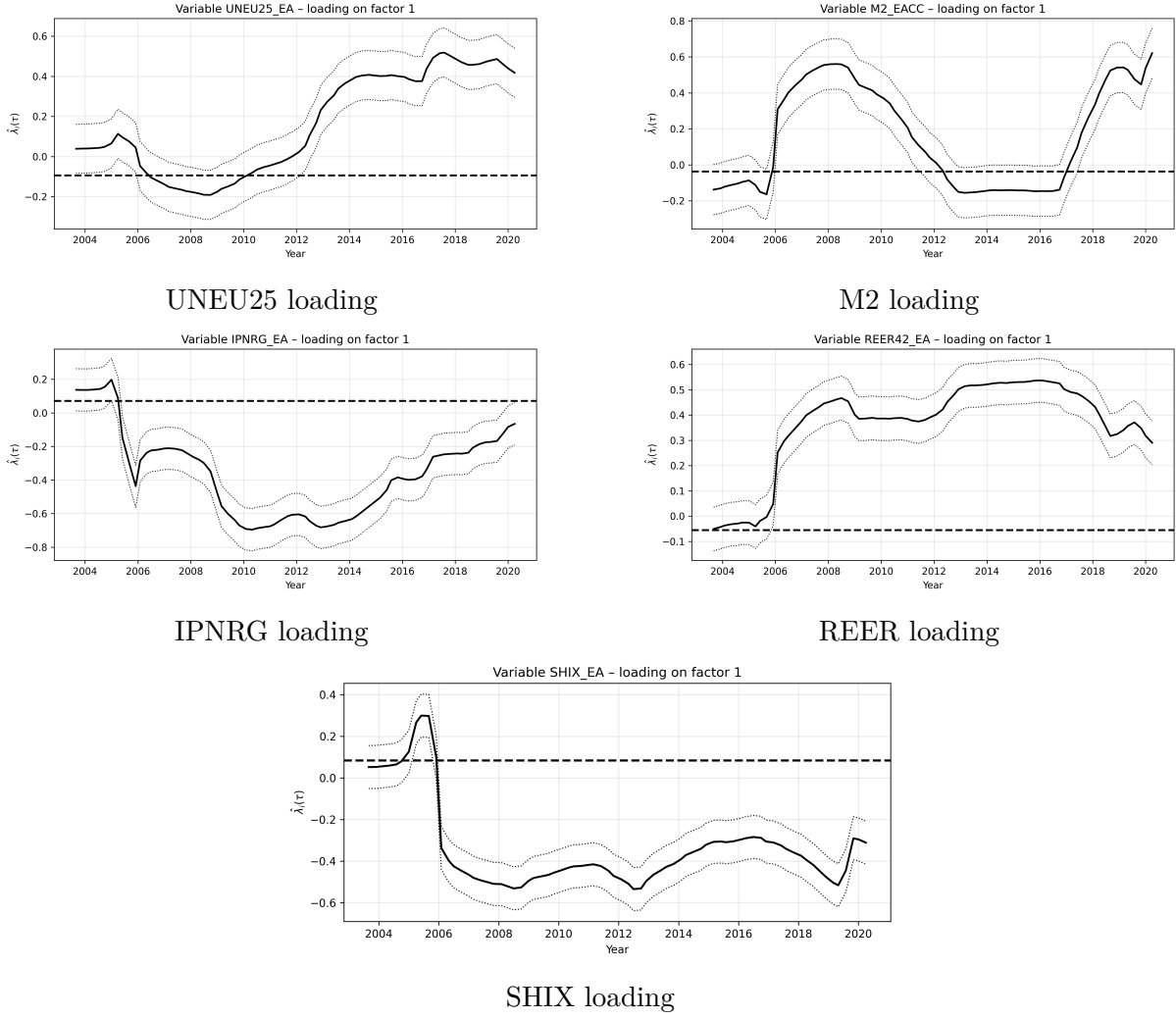


Figure 4: Loadings on the first factor

6.3.2 Second Factor

While F_1 reflects real economic activity, F_2 captures broad economic expectations, acting as a forward-looking factor since investment and monetary intentions usually precede changes in output or unemployment. “Economic sentiment” refers to the overall confidence or pessimism of consumers and firms regarding current and future economic conditions: high sentiment fosters spending and investment, while low sentiment leads to saving and sluggish growth.

The main loadings of latent variables such as **ICONFIX_EA** (-0.612), **ESENTIX_EA** (-0.610), **BCI_EA** (-0.606), and **SCONFIG_EA** (-0.550) indicate a strong negative correlation between Euro Area sentiment and F_2 . Conversely, unemployment indicators like **UNETOT_EA** and **UNE025_EA** have positive loadings (around 0.50), showing that higher confidence coincides with lower unemployment.

After a period of relative stability, confidence dropped sharply, reaching its lowest point in 2009 and recovering to baseline only after 2013. This aligns with the 2008 Lehman Brothers collapse, when global financial turmoil and uncertainty fueled risk aversion. Between 2013 and 2019, trade and industrial sentiment improved but remained fragile due to slow growth, gradually declining unemployment, and moderate inflation.

In 2020 this trend reversed with the outbreak of COVID-19, never returning to pre-crisis levels. The same pattern is visible in **SCONFIG_EA**, though its 2008 dip is milder, while the post-2017 fall is unprecedentedly sharp. Between 2007 and 2009, real estate collapsed but

government stimulus and low rates temporarily sustained investment. By contrast, the 2020 lockdown disrupted production and supply chains, pushing sentiment to record lows. Subsequent easing and stimulus led to a partial rebound, uneven across sectors.

Overall, the curve for **SCONFIG_EA** is smoother than that of **RTCONFIG_EA**, reflecting the industrial sector's alignment with broader cycles, whereas retail confidence reacts more quickly to short-term shocks such as the lockdown.

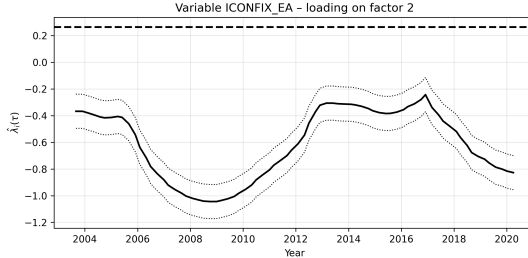


Figure 5: ICONFIX_EA loading on F2

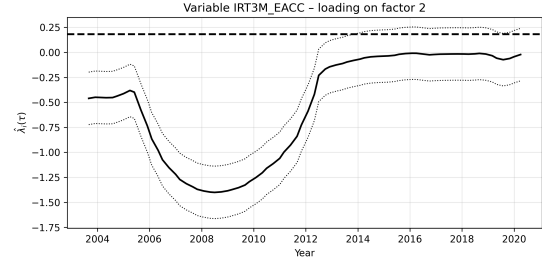


Figure 6: IRT3M loading on F2

Equally relevant indexes contributing to our analysis of the second factor are **IRT3M_EACC** (-0.529) and **IRT6M_EACC** (-0.515), interest-rate indicators that partly confirm the trend previously discussed above and provide additional insightful information for our analysis of time-varying loadings (Figure 2).

Their negative loadings suggest that as general sentiment improves, both three months (**IRT3M**) and six months (**IRT6M**) interest rates decrease – and vice versa. The strongest negative co-movement is again experienced around 2007–2009, when the ECB moved from tightening to emergency cuts and rates fell from around 4.25% to 1%. The 2006–2010 financial crisis, triggered by the U.S. subprime mortgage collapse, led to a severe credit crunch where the Fed aggressively cut short-term rates to near zero to re-stabilize the banking system.

After the global financial crisis, the loading rose steadily from around -1.5% in 2009 to nearly zero, marking a shift from a cyclical to a policy-driven dynamic. Before 2008, short-term interest rates tended to move counter-cyclically – falling when confidence weakened and rising as sentiment improved. In the post-crisis period, however, this link progressively vanished as the ECB adopted an ultra-accommodative stance. From 2014 onwards, with policy rates close to or even below zero, short-term rates ceased to reflect the state of the economy or the prevailing sentiment, remaining artificially low as a deliberate policy tool to sustain demand and anchor credibly expectations.

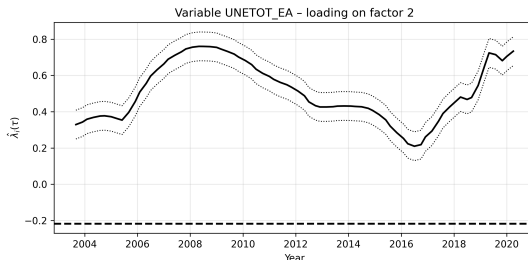


Figure 7: UNETOT_EA loading on F2

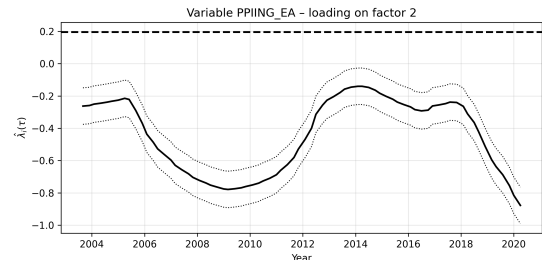


Figure 8: PPIING_EA loading on F2

From 2003 to 2020, the loading of unemployment on economic sentiment fluctuated markedly, reflecting how the link between joblessness and collective outlook evolved through major crises. The impact of unemployment on F_2 is captured by **UNETOT** (0.510) and **UNEU25** (0.498), both loading positively on the factor. During the two major crises, unemployment loadings rose sharply, showing an almost symmetric pattern to previous indicators. Between 2006 and 2012, the loading increased from about 0.35 to 0.8, indicating that pessimism and labor market

weakness became closely intertwined.

After 2008, loadings declined as sentiment recovered faster than employment, suggesting a temporary decoupling likely driven by policy support and slow labor adjustments. Confidence improved with Euro Area stabilization and quantitative easing despite persistent joblessness. Between 2016 and 2021, loadings rose again to around 0.7, reflecting the late recovery and the renewed sensitivity of sentiment to unemployment ahead of COVID-19. Following the pandemic, unemployment once more became a key driver of F_2 , signaling that confidence remained highly responsive to labor market fragility.

Lastly, the role of **PPIING**, a Producer Price Index measure, shows an average negative loading of -0.442 , implying that inflation generally moves opposite to sentiment. This inverse relationship strengthened from -0.3 to -0.8 between 2003 and 2008, during the global financial crisis, when rising input costs coincided with declining confidence. It weakened in the following years, as both sentiment and PPI stagnated, before turning sharply negative again between 2018 and 2020 (-0.9) amid the COVID-19 shock, when both collapsed simultaneously.

Interpretation of Factors 3–6

Factor 3 – Monetary and labour conditions: This factor is negatively correlated with both nominal (ERUS) and real (REER42) exchange rates, meaning that higher factor values correspond to a weaker euro. It also loads positively on unemployment and monetary aggregates (M1–M2), while confidence indicators move in the opposite direction. Overall, it captures phases of economic slack and monetary easing, when euro depreciation, rising unemployment, and liquidity expansion coexist with low confidence and weak activity.

Factor 4 – Goods and energy inflation: This factor shows strong positive loadings on consumer and energy price indices (HICP, PPI) and negative ones on industrial production and turnover in consumer goods. It captures episodes of supply-side inflation, where higher prices coincide with falling output and rising long-term interest rates. The combination of inflationary pressures and real contraction points to cost-push dynamics driven by energy and input shocks.

Factors 5–6 – Residual real and financial dynamics: The fifth and sixth factors are more difficult to interpret clearly. Factor 5 mixes energy-related price pressures with labour market slack and competitiveness, suggesting a residual cost-push component overlapping with the main inflation factor. Factor 6, instead, loads negatively and uniformly on industrial production, turnover and equity prices, hinting at a broad but less distinct real-financial cycle. Both likely capture secondary co-movements—sectoral or cyclical—rather than autonomous macroeconomic forces.

6.4 Out-of-sample performance (one-sided)

We emphasize that forecasting is not the primary objective of this study. The Time-Varying Factor Model is estimated in a two-sided framework, where both past and future information contribute to the extraction of latent factors. The one-sided out-of-sample (OOS) evaluation presented here is thus intended only as a robustness exercise, assessing whether the model retains reasonable predictive ability when estimated recursively using information available up to each τ .

In this strictly one-sided setting, the adaptive ABC selection does not outperform the fixed- r benchmark: mean and median ΔR^2 are negative (-0.031 and -0.035), and a paired t -test rejects equality ($t = -4.66$, $p = 0.0000$). For squared loss the evidence is weak: the average ΔMSE is slightly negative but not statistically different from zero ($t = 1.01$, $p = 0.3181$). In absolute terms, the ABC specification attains a mean R^2_{OOS} of 0.419 (min 0.232 , max 0.648) and a mean MSE_{OOS} of 0.363 (min 0.193 , max 1.498). The spike observed in the out-of-sample MSE is largely driven by strong shifts in local means within the one-sided windows, which inflate the absolute error whenever the forecast deviates even slightly from the true level. Since R^2 is a relative measure – normalized by the local variability – it is much less sensitive to level shifts and therefore provides a more reliable basis for comparing model performance across specifications.

These results indicate that allowing for time variation in factor dimension does not materially deteriorate the model's predictive accuracy. The modest differences observed are likely influenced by the fact that roughly half of the available observations are used for model estimation, while forecasts are generated for the subsequent 30% of the sample – a relatively short evaluation window that limits the potential benefit of adaptive selection.

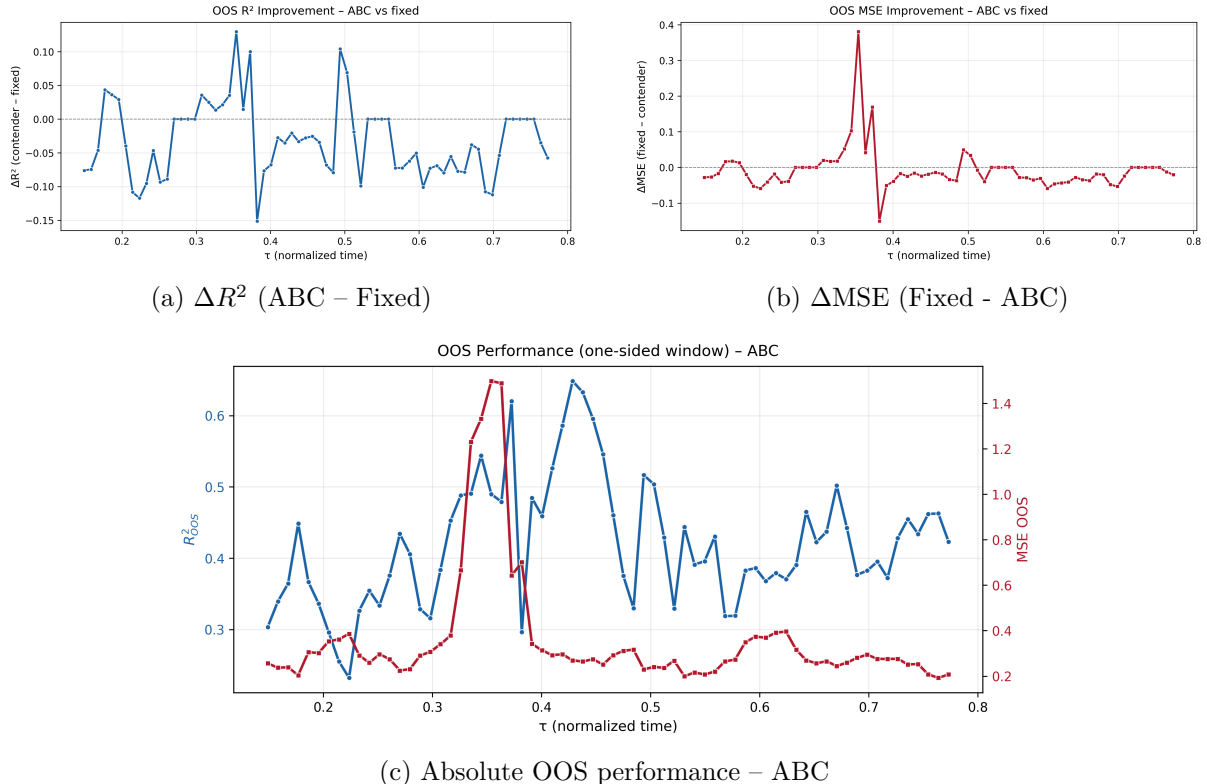


Figure 9: One-sided OOS evaluation. Panels (a)–(b) show differences vs a fixed- r benchmark; panel (c) reports absolute performance of the ABC specification.

Table 1: OOS comparison – ABC vs fixed selection and absolute OOS performance (one-sided)

Statistic	Value		
ABC vs Fixed (68 common τ)			
Mean ΔR^2	-0.031	Median ΔR^2	-0.035
Share($\Delta R^2 > 0$)	19.12%		
Mean ΔMSE	-0.007609	Median ΔMSE	-0.018637
Share($\Delta \text{MSE} > 0$)	19.12%		
Paired t-test ΔR^2	$t = -4.66, p = 0.0000$		
Paired t-test ΔMSE	$t = 1.01, p = 0.3181$		
Absolute OOS performance – ABC			
Mean R^2_{OOS}	0.419	Min	0.232
Max R^2_{OOS}	0.648		
Mean MSE_{OOS}	0.362886	Min	0.192510
Max MSE_{OOS}	1.497662		

7 Conclusions

The empirical analysis highlights the relevance of allowing for time variation in the factor structure. Compared to a static specification, the time-varying model captures more accurately the evolving relationships among macro-financial variables, which appear to change significantly in response to major economic and policy shocks. The evidence suggests that the common factors shaping aggregate comovements are themselves affected by these shocks, both in their strength and composition, reflecting the shifting nature of underlying economic forces.

In addition, the optimal number of factors is not constant over time: it tends to rise during episodes of heightened turbulence, such as financial or sovereign crises, when additional dimensions are needed to account for the complexity and interdependence of economic dynamics. Overall, these findings underline the importance of incorporating structural changes and regime-dependent behaviour when modeling macro-financial linkages in an evolving economic environment.

References

- Alessi, Barigozzi, C. (2010). Improved penalization for determining the number of factors in approximate factor models. *Statistics Probability Letters*, 80(23-24):1806–1813.
- Bai and Ng (2002). Determining the number of factors in approximate factor models. *Econometrica*, 70(1):191–221.
- Forni, M., Hallin, M., Lippi, M., and Reichlin, L. (2009). Opening the black box: structural factor models versus structural vars. *Econometric Theory*, 25(5):1319–1347.
- Hallin and Liška (2007). Determining the number of factors in the general dynamic factor model. *Journal of the American Statistical Association*, 102(478):603–617.
- Stock and Watson (2002). Forecasting using principal components from a large number of predictors. *Journal of the American Statistical Association*, 97(460):1167–1179.
- Su and Wang (2017). On time-varying factor models: Estimation and testing. *Journal of Econometrics*, 198(1):84–101.